in silico Plants, 2023, **5**, 1–13
https://doi.org/10.1093/insilicoplants/diad010
Advance access publication 16 August 2023
Original Research

Original Research

Development and stochastic validation of a parameterized model of maize stalk flexure and buckling

Michael Ottesen, Joseph Carter, Ryan Hall, Nan-Wei Liu and Douglas D. Cook*

Department of Mechanical Engineering, 701 E. University Parkway, Brigham Young University, Provo, UT 84602, USA

*Corresponding author's e-mail address: ddc971@byu.edu

Handling Editor: Xin-Guang Zhu

Abstract. Maize stalk lodging is the structural failure of the stalk prior to harvest and is a major problem for maize (corn) producers and plant breeders. To address this problem, it is critical to understand precisely how geometric and material parameters of the maize stalk influence stalk strength. Computational models could be a powerful tool in such investigations, but current methods of creating computational models are costly, time-consuming and, most importantly, do not provide parameterized control of the maize stalk parameters. The purpose of this study was to develop and validate a parameterized 3D model of the maize stalk. The parameterized model provides independent control over all aspects of the maize stalk geometry and material properties. The model accurately captures the shape of actual maize stalks and is predictive of maize stalk stiffness and strength. The model was validated using stochastic sampling of material properties to account for uncertainty in the values and influence of mechanical tissue properties. Results indicated that buckling is influenced by material properties to a greater extent that flexural stiffness. Finally, we demonstrate that this model can be used to create an unlimited number of synthetic stalks from within the parameter space. This model will enable the future implementation of parameter sweep studies, sensitivity analysis and optimization studies, and can be used to create computational models of maize stalks with any desired combination of geometric and material properties.

KEYWORDS: Lodging; maize; modelling; morphology; parameterized; stalk.

1. INTRODUCTION

Maize stalk lodging (wind-induced failure of the stalk) represents a major source of loss for farmers (Flint-Garcia *et al.* 2003; Duvick 2005). In late-season lodging, maize stalks fail due to localized (Brazier) buckling, which manifests as a characteristic 'creasing' of the stem just above a node (Robertson *et al.* 2015*b*). The term 'buckling' refers to a sudden change in shape of a structural component under loading, often resulting in collapse. Brazier buckling involves localized shape change and should not be confused with the more well-known Euler buckling, which applies to large-scale buckling of columns. The creasing of a drinking straw that occurs when the straw is gently bent is the most commonplace example of Brazier buckling.

Stalk bending strength refers to the maximum bending load that can be applied to a stalk prior to the onset of buckling. Stalk bending strength is a major factor in determining lodging resistance and has been shown in both empirical and computational studies to be closely related to stalk morphology (Gomez *et al.* 2017; Robertson *et al.* 2017, 2022). In this paper, 'strength' always refers to ultimate bending strength. Tissue strength is also of interest in predicting ultimate strength but it is not addressed in this study.

It has been proposed that relatively minor changes in stalk morphology might lead to significant increases in stalk strength (Von Forell *et al.* 2015). To improve maize stalk strength through breeding and/or biotechnology, two key advances are needed: (1) the ability to rapidly measure the morphology of the maize stalk and (2) insight into which morphological features are most closely related to maize stalk strength. This study addresses the second need by developing a method for manipulating the morphology of maize stalks.

The finite element method has previously been used to create models of maize stalks (Von Forell *et al.* 2015; Stubbs 2019; Stubbs *et al.* 2019, 2020, 2022). In the broader biomechanics literature, the finite element method is a powerful and pervasive tool. In human biomechanics, the finite element method has been used to study a wide range of topics, including the human knee, foot, pelvis, liver, brain, heart arteries and many others (Besnault *et al.* 1998; Erdemir *et al.* 2006; Andersen *et al.* 2021). There are two primary methods used to create specimen-specific

models. First, image-based modelling is commonly used to create models directly from imaging data such as CT or MRI scans. Such models typically provide very high geometric fidelity and are thus very close approximations to the specimens from which they were derived. These models typically require a significant amount of manual segmentation and modelling effort by a trained technician (Patil and Deore 2013). As a result, these models are costly and time-consuming to create. Moreover, once created, the geometry of these models is essentially static and cannot be manipulated to investigate the influence of geometry (Cook *et al.* 2014).

To overcome these limitations, parameterized modelling schemes have been developed. Parameterized models typically utilize geometric features and/or landmarks of the system to be modelled (Maurel *et al.* 1997; Danelson *et al.* 2009; Sigal *et al.* 2010). Parameterized models provide good approximations of the geometry of the desired specimen and provide control over model shape through the adjustment of model parameters. This approach dramatically expands the utility of these models by enabling parametric studies, sensitivity studies and optimization studies. However, the parameterization scheme typically requires geometric approximations, so parameterized models do not allow the same level of geometric detail as image-based models.

Ottesen *et al.* (2022) used machine-learning techniques to develop a two-dimensional parameterization of the maize cross-section. The Ottesen model was based on a simple ellipse as the exterior boundary of the stalk and an offset ellipse as the boundary between rind and pith tissue. Finer geometric features such as the ear groove and various types of asymmetries in the model were captured using principal components derived from actual cross-sections. Ottesen *et al.* reported that any desired level of geometric fidelity could be obtained by adding additional principal components. The model was validated under a variety of loading cases, including bending, torsion, axial tension/compression and transverse compression. Notably, the ellipse alone (no principal components) provided high predictive accuracy in all cases and required just three geometric parameters: major diameter, minor diameter and rind thickness. The primary limitation of the Ottesen model is that it did not account for axial variation of the maize stalk.

A fully parameterized, three-dimensional model of the maize stalk would allow control over individual geometric features. Such a model could be used to determine which geometric features of the maize stalk are most closely related to maize stalk strength. It could also be used to determine the optimal stalk architecture that balances biomass with both strength and flexibility. The purpose of this study was to develop a three-dimensional parameterized model of the maize stalk. We validated this model in three ways. First, by assessing its geometric similarity to original stalks. Second, by determining the ability of this model to accurately predict flexural stiffness, and third, by assessing the ability of this model to predict the strength of maize stalks. In contrast with prior studies, stochastic (randomized) variation in material properties was used to account for the influence of material uncertainties on the validation process. The resulting model opens many avenues for advanced computational analyses of maize stalk strength.

2. METHODS

2.1 Overview

This study is based on two important data sources from previous studies: (1) CT scans of maize stalks and (2) corresponding physical 3-point bending tests (Robertson *et al.* 2016, 2017). Previous research has confirmed that 3-point bending tests can be used to assess stalk bending strength because these tests induce the same type of buckling failure observed in natural lodging (Robertson *et al.* 2014, 2015*a*, *b*)

Figure 1 shows the physical testing arrangements along with sample CT scan images. This figure also depicts the creation of CT-based finite-element models (Stubbs *et al.* 2022), the use of CT scan data to create 2D parameterized models (Ottesen *et al.* 2022) as well as the 3D parameterized models developed in this study.

2.2 Empirical data

Three-point bending tests and the CT-scanning process were described in previous studies (Robertson *et al.* 2016, 2017). Briefly summarized, approximately 900 maize stalks were scanned and then tested in 3-point bending. During bending tests, stalks were gradually loaded until localized buckling occurred. This testing approach provided empirical measurement of two mechanical features of each stalk: flexural stiffness (also known as flexural rigidity) and ultimate bending strength. CT scans provided detailed three-dimensional data on each maize stalk at a resolution of 78 μm per voxel. This resolution typically results in over 200 pixels across the minor diameter of the stalk and over 100k pixels within each cross-section. Representative CT cross-sections are shown in Fig. 1.

The CT data for each stalk consisted of approximately 1500 cross-sectional images. Because adjacent images were nearly identical to each other, a non-uniform sampling scheme was used. In this scheme, 46 cross-sectional images were extracted from each stalk using higher sampling density near the node and lower sampling density in the internodes. The 46 sampling points can be seen as light grey vertical lines that intersect the longitudinal CT cross-section image in Fig. 1.

2.3 Parameterization method

2.3.1 *Ellipse-based axial sweep*

Each cross-section of each stalk was approximated as an ellipse as described previously (Ottesen *et al.* 2022). The interior ellipse was offset from the exterior boundary by the rind thickness. The rind thickness was determined as the average distance between the interior and exterior boundaries of the maize stalk cross-section (Robertson *et al.* 2017). This process produced profiles for the major diameter a, minor diameter b and rind thickness t as functions of axial location z for 900 individual stalks. For each individual stalk, these three profiles define a 3D shape that closely approximates the original stalk geometry. Figure 2 provides an illustration of the swept-ellipse geometry.

2.3.2 *Parameter profiles*

The profiles, $a(z)$, $b(z)$ and $t(z)$, exhibited distinct features that were present in virtually all stalks. Figure 3 depicts the data distributions for each parameter profile, with dark shading indicating high data density and light shading indicating low data density. The solid white line in the centre of each chart represents the average profile.

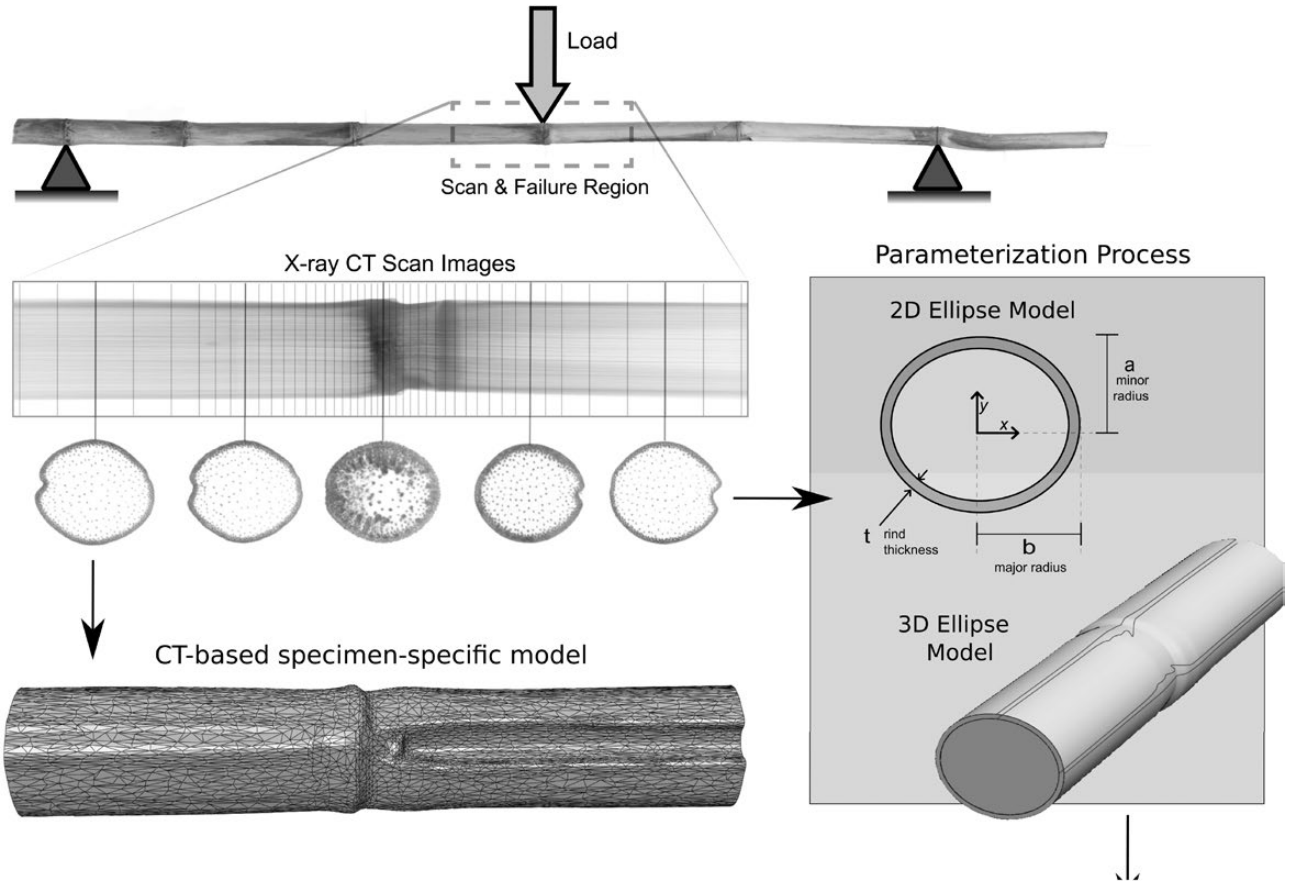

Figure 1. Overview illustration showing the relationships between physical experiments, CT-scan data and model types discussed in this study. Figure adapted with permission from Robertson *et al.* 2017.

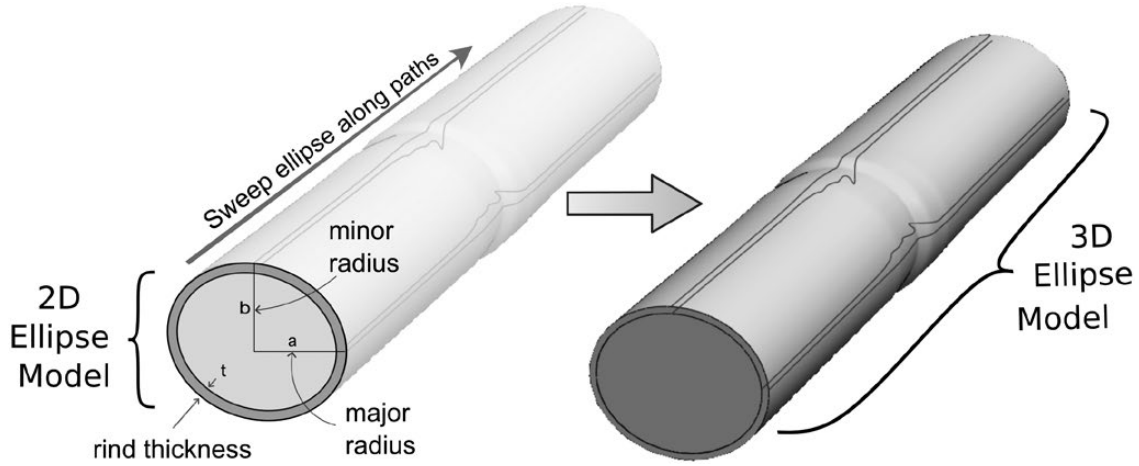

Figure 2. Ellipse sweep model, depicting the 2D ellipse, ellipse parameters, parameter profiles and the resulting 3D ellipse model.

2.3.3 *Profile parameterization*

Machine-learning techniques and landmark identification were used to parameterize the essential features of each parameter profile. This was accomplished by iterating between principal component analysis (also known as empirical eigenfunction analysis) and landmark identification. Early attempts applied principal component analysis to each profile separately or to all three profiles simultaneously. Although this approach does provide an immediate parameterization based on variance decomposition (Jackson 2003), this method does not enable independent control of physical features and was therefore abandoned. For similar reasons, polynomial-based regression approaches were excluded because this provides no physical connection between coefficient values and physical features of the corn stalk.

Landmarks were selected based on consistent and distinctive features, which were found to be present in virtually all

stalk profiles. Most landmarks were peaks or valleys in the respective profiles. Each landmark was defined by two coordinate values. The first coordinate was the axial location z. The z-axis origin was defined as the central peak in the rind thickness profile. This feature was chosen as a reference because it was (a) the most distinct of all landmarks and (b) identifies the centre of each node (the dividing line between stalk segments). The second coordinate was the perpendicular distance of each profile (major diameter, minor diameter and rind thickness) from the z-axis. Figure 4 shows representative profiles with landmarks indicated by dots. Each profile contains six distinct landmarks: two endpoints and four peaks/valleys. Supplementary information included with this paper includes animations showing the degrees of freedom controlled by each parameter.

Custom software was developed to automatically identify these landmarks for each of the 980 × 3 = 2940 profiles used in the study. Principal component analysis was then used to capture and parameterize the transition patterns between landmarks. A local, normalized coordinate system was defined for each neighbouring pair of landmark points. The original and subsequent coordinate systems are shown in Fig. 3. The transverse values retained their original units but the transverse value of the first landmark was subtracted so that the coordinate value of the first landmark was (0,0). The local coordinate system is shown in Fig. 3B.

Next, the landmark points were connected in the local coordinate system by a straight line. The final 'subtracted' coordinate system captures the vertical distance between the line connecting the landmarks and individual points on the profile. The subtracted coordinate system is shown in Fig. 5C.

These coordinate transformations can be expressed mathematically as follows, where each of the symbols is defined as shown in Fig. 5, the subscript i is the index associated with landmarks, and braces, {}, indicate vectors of values in the specified coordinate systems:

$$\{z_{\text{local}}\} = \frac{\{z_{\text{orig}}\} - L_z^i}{L_z^{i+1} - L_z^i} \tag{1}$$

$$\{y_{\text{local}}\} = \{y_{\text{orig}}\} - L_y^i \tag{2}$$

$$\{z_{\text{sub}}\} = \{z_{\text{local}}\} \tag{3}$$

$$\{y_{\text{sub}}\} = \{z_{\text{local}}\}\left(L_y^{i+1} - L_y^i\right) - y_{\text{local}} \tag{4}$$

Principal component analysis was then performed on the subtracted coordinate system data, y_{sub} and z_{sub}. Since all subtracted profiles have values of zero at each landmark, all empirical eigenfunctions also have zero values at landmarks. This allows empirical eigenfunctions to be added directly to the straight line connecting each pair of landmarks. The empirical eigenfunctions connecting landmarks can then be varied by linearly scaling the empirical eigenfunctions, $\{e_k^i\}$ using scaling coefficients, c_k^i. Note that eigenfunctions are represented as vectors. The parameterization of each parameter profile between landmarks i and $i + 1$ is thus given as follows:

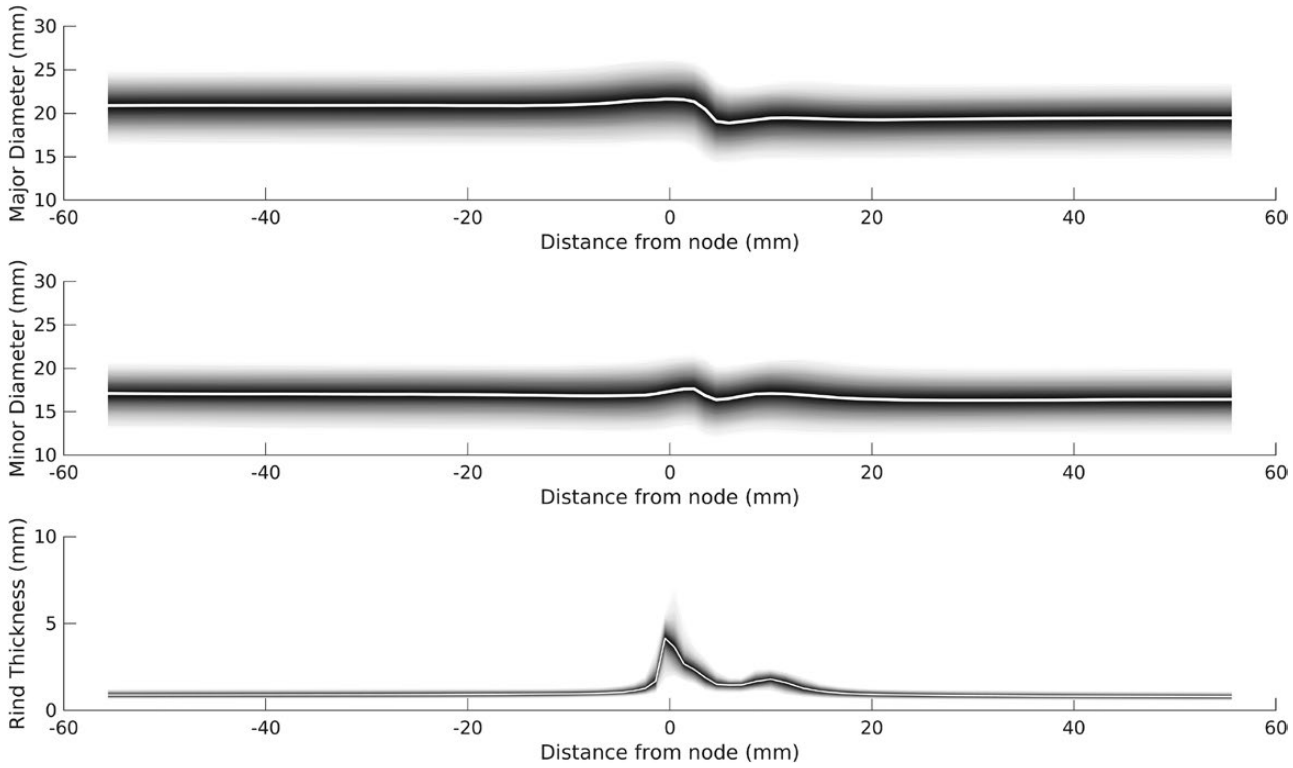

Figure 3. Data distributions for major diameter, minor diameter and rind thickness profiles. Darkness intensity represents data density. The central white line represents the average profile.

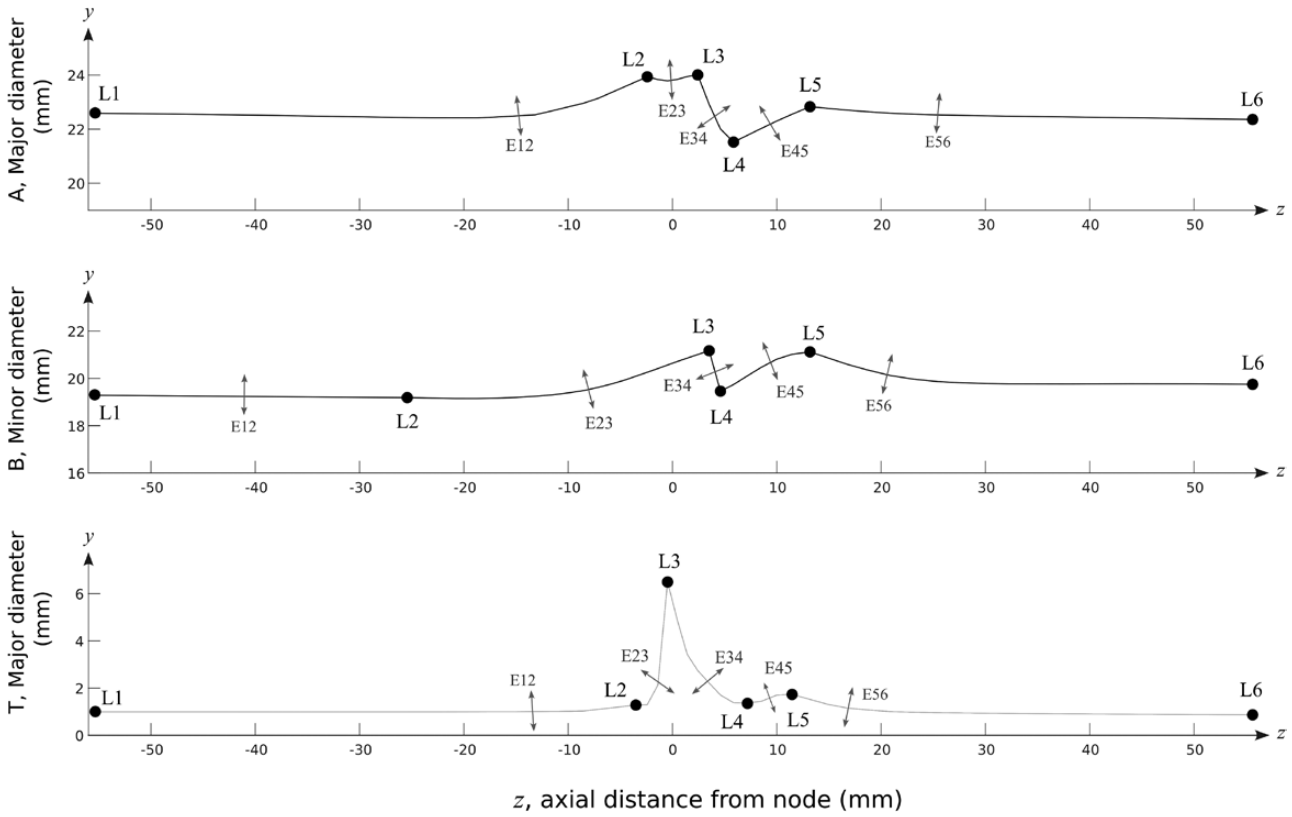

Figure 4. Representative profiles of the major diameter (top), minor diameter (middle) and rind thickness (bottom). Landmarks (L) are indicated by black dots and the influence of each eigenfunction (E) is represented by a double-headed arrow. All dimensions are in mm. Supplementary animations have been provided to aid in interpreting these parameters.

$$\left\{y^i_{\text{par}}\right\} = \left(\frac{L^{i+1}_y - L^i_y}{L^{i+1}_z - L^i_z}\right)\left\{z^i_{\text{orig}}\right\} + L^i_y + \sum_{k=1}^{N} c^i_k \left\{e^i_k\right\} \quad (5)$$

Here, $\{y_{par}{}^i\}$ represents the vector of parameterized sample points defining the parameter profile between landmarks i and $i + 1$. The summation term represents the series of empirical eigenfunctions while the other terms on the right-hand side represent a straight line connecting landmarks i and $i + 1$. The index k refers to the series of empirical eigenfunctions. The first principal component (or empirical eigenfunction) typically captured approximately 96 % of the variation in a transition pattern. This approach allows any desired geometric fidelity to be captured by simply adding additional eigenfunction terms.

To summarize, the parameterized model of maize stalk morphology consists of an axially varying elliptical cross-section. The variation in ellipse shape is defined by three parameter profiles: major diameter, minor diameter and rind thickness (Fig. 2). Each of these profiles is defined by six landmarks (Fig. 4). Straight lines connect adjacent landmarks and transition patterns between landmarks are captured by linearly scaled empirical eigenfunctions (Fig. 5). Any number of empirical eigenfunctions can be used in this scheme, which allows for complete reconstruction of the axial patterns of ellipse profiles when all eigenfunctions are utilized. We found that the first empirical eigenfunction captured the vast majority of geometric variation, so only one eigenfunction was used in this study. With a single empirical eigenfunction, the shape of the parameterized 3D model is defined by 51 parameters, each of which can be independently adjusted/controlled. These parameters are shown in Fig. 4 and listed in **Supporting Information—Table S1** that accompanies this paper.

2.4 Generating parameterized models

The parameterized model provides the ability to fit the parameterized model to actual maize specimens. The parameterized model was fit to each of the original 900 maize stalks in the database. Once the fitting process was completed, a subset of corresponding finite-element models was created.

It is also possible to use the parameterized model to generate an arbitrary number of novel 'synthetic' stalk models. This was accomplished using the normal copula method (McClarren *et al.* 2018). This method produces a synthetic population in which the mean values, standard deviations, correlations and parameter distribution shapes of the synthetic population match those of the original data set. This approach preserves key relationships between parameters. Synthetic models can also be generated to meet any arbitrary set of pre-determined statistical attributes. The methods for model fitting, modification and generating synthetic stalks are described in the following sections.

2.5 Creating specimen-specific parameterized models

Several steps were required to fit the parameterized model to an individual stalk specimen. First, ellipses were used to capture

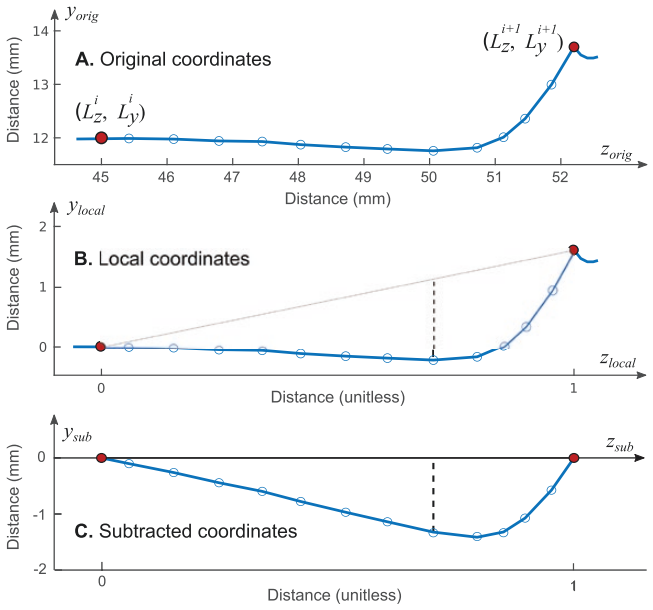

Figure 5. Coordinate systems used to calculate the principal component patterns between landmark points. A: original coordinates, B: local coordinates, C: subtracted coordinates.

each cross-section of the original stalk geometry. The ellipse fitting resulted in axial profiles for the major diameter, minor diameter and rind thickness similar to those shown in Fig. 4. The landmarks were then identified. The coordinates of landmark points provided 36 of the 51 parameters [**see Supporting Information—Table S1**].

Next, transitions between each pair of landmark points were captured using empirical eigenfunctions. Each transition pattern between landmark points was converted to local and subtracted coordinate systems as described in Equations (1–4). This produced a vector of $\{y_{sub}\}$values for each transition pattern. The following equation was then used to approximate $\{y_{sub}\}$:

$$\{y_{sub}\} = [E]\{c\} + \{\varepsilon\} \quad (6)$$

Here, $[E]$ is a matrix of the eigenvectors to be included in the parameterization, {c} is a vector of coefficients and {ε} is a vector of residuals. The least-squares method was used to obtain the coefficient vector {c}, which was then used in Equation (4) to parameterize each profile.

2.6 Creating a population of synthetic models

The Gaussian copula method was used to create a population of synthetic models that had the similar statistical characteristics as the original set of 900 stalks. First, the parameterized model was fit to all 900 stalks in the original data set. This produced a 900 × 51 matrix of parameter values. This matrix was then used to calculate the 51 × 51 correlation matrix, R as well as empirical cumulative density functions for each parameter.

The Gaussian copula is formed by performing Choelesky factorization on the R matrix to obtain a lower diagonal matrix L, sampling a set of standard normal random values, and then mapping those values into new coordinates according to the relationships between variables captured by R, and probability density characteristics captured by the cumulative density functions. This process is described in more detail in McClarren *et al.* (2018).

This process created a new population of N stalks. The value N can be set to any desired value. The quality of Gaussian copula was assessed by creating a new synthetic set of 900 stalks. The mean and standard deviation for both the original and synthetic sets were compared. The correlation matrix of the synthetic set was also compared term-by-term with the original correlation matrix. Finally, the empirical cumulative density functions of the synthetic stalk set were compared term-by-term to the original empirical density functions.

2.7 Finite element models

The finite element method was used to create parameterized models of maize stalks. Models were generated using Abaqus/CAE 2022 by defining the appropriate material properties, mesh and boundary conditions, as described in the following sections.

2.7.1 Mesh

The mesh of each parameterized finite element model was broken into three sections: top end, node region and bottom end. The node region spans 10 mm with the fixed boundary condition in the centre. The top and bottom ends were meshed using a hexahedral mesh due to the simplicity/regularity of the geometry in this region. The nodal region was meshed using a tetrahedral mesh to account for the more complex internal geometry of this region (see Fig. 6). The rind was given high mesh density, while the pith was given low mesh density. This was done as most stresses in bending occur in the rind. An extensive mesh convergence study was performed to ensure that this mesh produced mesh-converged results.

2.7.2 Boundary conditions

The boundary conditions for the parameterized finite element 3D model match the shear and moment loads that were present upon the modelled segment during physical 3-point bend testing. This approach has been previously used and validated (Stubbs *et al.* 2022). Because the finite element models only account for a portion of the stalk, as shown in Fig. 1, the relevant shear and moment loads were applied to the end faces of the finite element model. The loading anvil at the centre of the stalk was held stationary with no degrees of freedom allowed at the point of contact between the anvil and the stalk. This boundary condition essentially prevents the model from rotating or translating in an undesired manner due to numerical round-off error. This same approach was used in a previous study (Stubbs *et al.* 2022). The expressions for shear and moment values are provided in Table 1 and the diagram in Table 1 shows these applied loads. Using the measured test values, the forces and moments for each finite element model were calculated using the equations in Table 1. In the finite element model, the central anvil of the finite element models was assumed to be fixed at six degrees of freedom.

2.7.3 *Mechanical tissue properties*

Both pith and rind tissues are characterized by fibres, which run longitudinally through the stalk. Plant tissues typically experience low levels of strain. As a result, both rind and pith tissues were modelled as linearly elastic transversely isotropic, as has been done in several previous studies (Von Forell *et al.* 2015; Stubbs *et al.* 2018, 2022). This material model requires five independent material properties for each tissue type, consisting of the modulus of elasticity in the fibre direction (E_3), the modulus of elasticity in the transverse plane (E_1 and E_2), the shear modulus in the fibre direction (G_{13} and G_{23}), the shear modulus in the transverse plane (G_{12}) and Poisson's ratio (ν). Currently, only E_1, E_2 and E_3 in the rind as well as E_1 and E_2 in the pith have been measured for maize tissues (Zhang *et al.* 2016; Al-Zube *et al.* 2017, 2018; Stubbs *et al.* 2019, 2020).

2.7.4 *Stochastic sampling of material property values*

Because not all the properties of maize tissue have been measured experimentally, some estimation is always required to obtain a full set of material properties. In previous studies, these estimates have had a limited scope: typically a single estimate was used for all other tissues (Von Forell *et al.* 2015; Stubbs *et al.* 2018, 2022) An unnaturally low level of biological variation in models can obscure the influence of material properties (Cook *et al.* 2014). In contrast, a direct treatment of variation and uncertainty provides much more reliable insights (Nelson *et al.* 2019).

In this study, realistic ranges were estimated for all material properties. Values for individual models were randomly sampled to account for the fact that these material properties are subject to significant levels of uncertainty. While many mechanical properties of maize tissues have not been measured, the relevant properties have been measured for many varieties of wood, both hardwood and softwood (Green *et al.* 1999). The longitudinal modulus of elasticity across many wood species has been reported by Green *et al.* as ranging from 4 to 16 GPa. This range corresponds almost exactly to the range reported by Al-Zube *et al.* (2018) for maize rind tissue: 3–17 GPa. Estimates for ranges of the missing maize material properties were based on the ranges and ratios of the same material properties reported for wood (Green *et al.* 1999). To aid in this process, we also referred to thermodynamic constraints, which exist when using a transversely isotropic material model. These constraints are (Lempriere 1968):

$$G_{12} = \frac{E_1}{2\left(1 + \nu_{12}\right)} \tag{7}$$

$$0 \leq \nu \leq 0.5 \tag{8}$$

Here, ν_{12} describes the relationship between passive strain in the 1 direction due to applied strain in the 2 direction.

The most important material property of maize stalks is the longitudinal modulus of the rind (Ottesen *et al.* 2022). In this study, the longitudinal modulus of the rind was measured directly for each specimen using the bending test method described in Al Zube *et al.* (2018). The remaining properties were randomly sampled from the ranges provided in Table 2. Normal distributions were used where possible. If insufficient information was available, uniform distributions were used.

2.7.5 *Finite element analyses*

Two analyses were performed for each model: flexural stiffness and linear buckling analysis. The flexural stiffness of the model was obtained using a static structural analysis. The force/deformation relationship from simulations was used to calculate an equivalent flexural stiffness, which was then compared to the measured value of flexural stiffness. Critical buckling loads were obtained using a linear buckling analysis. This type of analysis solves for instabilities in the structure and can be used for traditional column buckling or localized buckling. In this study, linear buckling analysis provided the load at which localized buckling instabilities occurred. This load represents an estimate

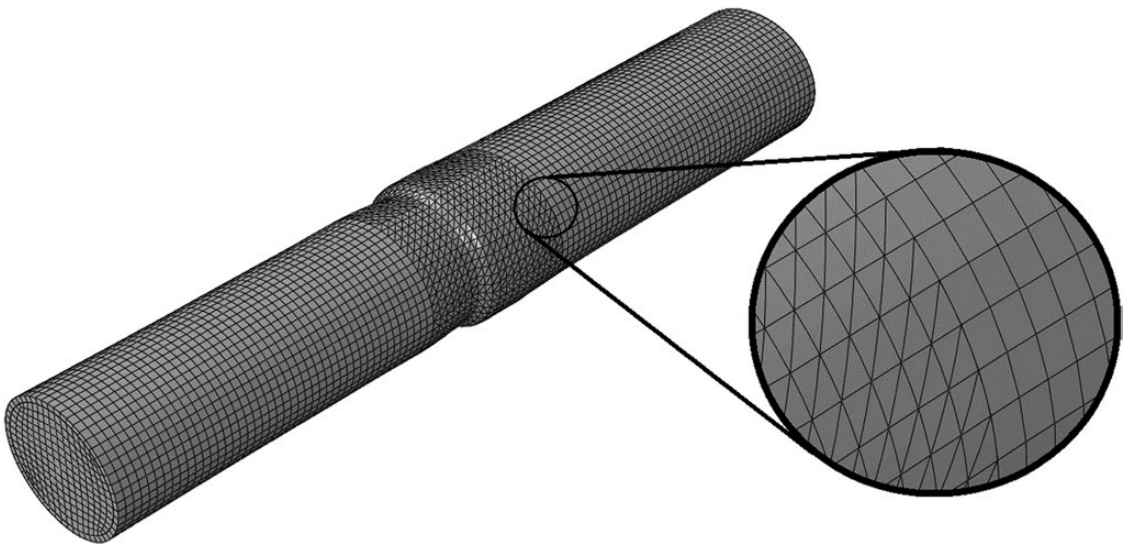

Figure 6. Isometric view of the finite element model and mesh. Enlarged section shows the transition from tetrahedral to hexahedral elements.

of the ultimate bending strength of the stalk. It should be noted that linear buckling analysis always overpredicts ultimate bending strength, but it is computationally much more efficient than dynamic explicit analyses (Xu *et al.* 2013; Bolton 2020). Both flexure and linear buckling methods have been previously validated for this purpose (Stubbs *et al.* 2022).

2.8 Model validation

2.8.1 *Cross-fold validation of parameterization method*

When using machine-learning methods, a portion of the data is used to train the model, with the remaining data held in reserve for validation of the model. The geometric maize stalk data used in this study was obtained from five different hybrid varieties. As these varieties are genetically distinct, the hybrid type was used as the basis for partitioning between training and validation sets. Rather than arbitrarily choosing certain hybrids for training and others for validation, we used the more robust cross-fold validation approach to investigate all possible training/validation combinations (Kolodiazhnyi 2020). In each training/validation set, the training set was composed of four hybrids with the remaining hybrid used for validation. Cross-validation consisted of repeating this process five times (one for each hybrid was used as the validation set).

Model validation was quantified by computing the R^2 value between validation set parameter profiles and the corresponding 'fit' obtained when using the model derived from the training data. This was performed for each stalk in the validation set and the profiles obtained after fitting the stalk with the model.

2.8.2 *Validation of finite element model predictions*

Finite element models were validated by comparing their predictions to the corresponding empirical test data (flexural stiffness and ultimate strength). Each parameterized specimen-specific model was created by fitting the parameterized ellipse model to the geometry of the corresponding CT scan. The specimen-specific longitudinal modulus of the rind (E_3) was also obtained from experimental test data. To account for uncertainty in the remaining material properties, 10 versions of each specimen-specific model were created. Each version utilized the same geometry and rind modulus, but different random values of the remaining material properties. This approach helps ensure that the validation results are not an artefact of a narrowly specified set of material properties.

Table 1. Loads applied to the finite element model.

Load type	Bottom face	Top face
Force	$F_a = \frac{M_{\text{fail}}}{A}$	$F_b = \frac{M_{\text{fail}}}{B}$
Moment	$M_a = \frac{A-a}{A} M_{\text{fail}}$	$M_b = \frac{B-b}{B} M_{\text{fail}}$

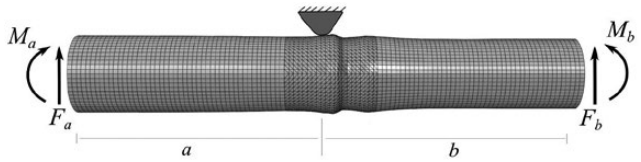

A	Distance between left-hand support and applied load in the 3-point bending test
B	Distance between right-hand support and applied load in the 3-point bending test
M_{fail}	Maximum bending moment applied during physical 3-point bending tests

3. RESULTS

3.1 Geometric cross-validation

The parameterized model geometry was compared to the actual stalk geometry by comparing actual profiles for major diameter, minor diameter and rind thickness to their parameterized model counterparts. For all five hybrids and across all three profiles, the R^2 values between original profiles and the parameterized profiles averaged 0.96 with the lowest value across all hybrids and profiles being 0.91. This indicates that the parameterization approach that has been developed is sufficiently flexible to accurately capture a range of maize stalk geometries. It should be noted here that each hybrid was grown at a wide range of planting densities and that planting density is known to have a strong effect on stalk morphology (Jun *et al.* 2017; Sher *et al.* 2017). The cross-validation statistics across validation sets are provided in Table 3.

3.2 Model creation time

The parameterized model automates the process of model creation, allowing models to be created programmatically instead of manually. The previous method required CT scanning and manual processing of the CT data to create each finite-element model. Including scanning time and manual manipulation of

Table 2. Summary of methods for obtaining material properties for finite element models. All modulus values are in GPa. Poisson's ratio values are unitless. Sampling distributions are specified as pairs. Normal distribution: (mean, standard deviation); uniform distribution: (lower bound, upper bound).

Property	Method	Distribution	Pith	Rind	Source
E_1, E_2	Random sampling	Normal	(0.026, 0.01)	(0.85, 0.39)	Stubbs *et al.* (2020)
Rind E_3	Specimen-specific	Empirical	n/a	Specimen-specific	Al-Zube *et al.* (2018)
Pith E_3	Random sampling	Normal	(0.05, 0.45)	n/a	Sutherland *et al.* (in review)
G_{12}	Calculated	n/a	$\frac{E_1}{2(1+\nu_{12})}$		Theory
G_{13} and G_{23}	Random sampling	Uniform ratio	(0.03× E_3, 0.21× E_3)		Green *et al.* (1999)
ν_{12}	Random sampling	Uniform	(0.2, 0.45)		
ν_{13} and ν_{23}	Random sampling	Uniform	(0.009, 0.086)		

data, this process required approximately 45 min per model/specimen.

The parameterized model is capable of building models at a rate of 40 s per model. This is 70× faster than previously possible and no manual model manipulation is required. Within a few minutes, the computer code that controls the model building process can be programmed to create hundreds or thousands of models. Model solve time is unchanged with respect to prior models. Using a Dell Precision 5820 Tower Workstation, each flexural analysis required 30 min of solving time and each buckling analysis required 90 min. Excluding mesh convergence, the results described below represent the creation and analysis of 1160 unique finite-element models.

3.3 Predictive accuracy of finite-element models

Direct comparisons between experimental results and simulated behaviour were performed to assess the validity of the parameterized model. A set of 59 stalks were randomly selected from the original set of 900 tested stalks. For each of these stalk geometries, a sample of 10 replicates were created, each having a unique set of plausible material properties. This resulted in 590 unique finite-element models. Across the 590 simulation results, predicted flexural stiffness compared very favourably to the measured flexural stiffness, with an R^2 value of 0.97 and a best fit line of slope 1.11. The average response across all replicates was calculated for each stalk geometry and also compared to measured flexural stiffness values. Both data sets are shown graphically in Fig. 7. Random variations in material properties had a relatively minor influence on the predicted values of flexural stiffness. This effect was quantified using variance decomposition. Only 1 % of the total variance was due to variations in material properties. This suggests that flexural stiffness is primarily dependent upon geometry and the longitudinal modulus of the rind (which was not varied because it was measured for each specimen).

A similar comparison was performed for the prediction of ultimate bending strength, which was assessed using linear buckling analysis. It is well known that linear buckling analysis tends to overpredict actual buckling loads (Xu *et al.* 2013; Bolton 2020). In a previous study using CT-based maize stalk geometries, linear buckling analysis was correlated with ultimate strength, but overpredicted it by a factor of approximately 10× (Stubbs *et al.* 2022). In this study, linear buckling results were also well correlated with ultimate strength but a more moderate overprediction of about 5× was obtained. Results for the full set of simulated stalks as well as replicate means are shown graphically in Fig. 8. With material variation included, the R^2 value between simulations and test results was 0.56. With material variation excluded (replicate averaging), the R^2 value between simulations and test results increased to 0.73.

Variation in material properties had a very noticeable influence on predicted ultimate strength. Using variance decomposition, it was found that 20 % of the variation in predicted

Table 3. Cross-validation R^2 values between the CT-based profile and corresponding parameterized models. Sample sizes varied between sets. The smallest sample size was n = 188.

	Profile			
Validation set	**Major diameter**	**Minor diameter**	**Rind thickness**	**Hybrid averages**
Hybrid 1	0.98	0.94	0.97	0.96
Hybrid 2	0.97	0.90	0.98	0.96
Hybrid 3	0.99	0.91	0.98	0.96
Hybrid 4	0.98	0.94	0.99	0.97
Hybrid 5	0.99	0.94	0.98	0.97
Averages	0.98	0.93	0.98	0.96

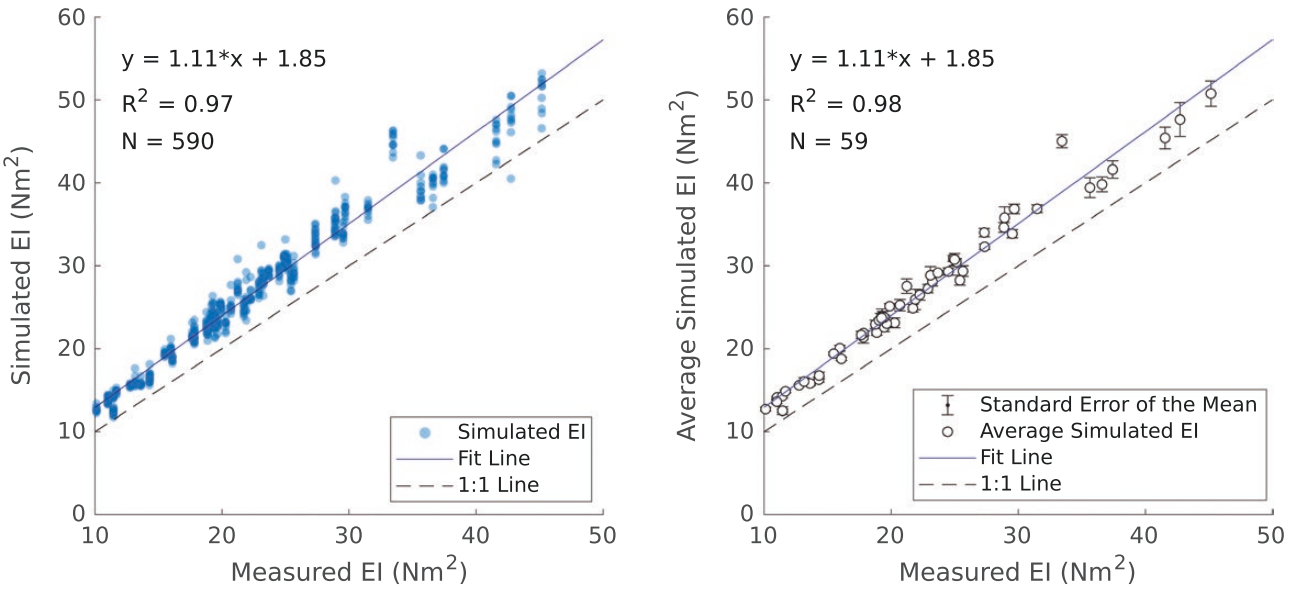

Figure 7. Comparisons between measured flexural stiffness (horizontal axis) and predicted flexural stiffness (vertical axis). The left-hand panel depicts the individual values obtained through random sampling of material properties. The right-hand panel shows the average response of each individual stalk. Error bars represent 95 % confidence intervals on the mean value of each distribution.

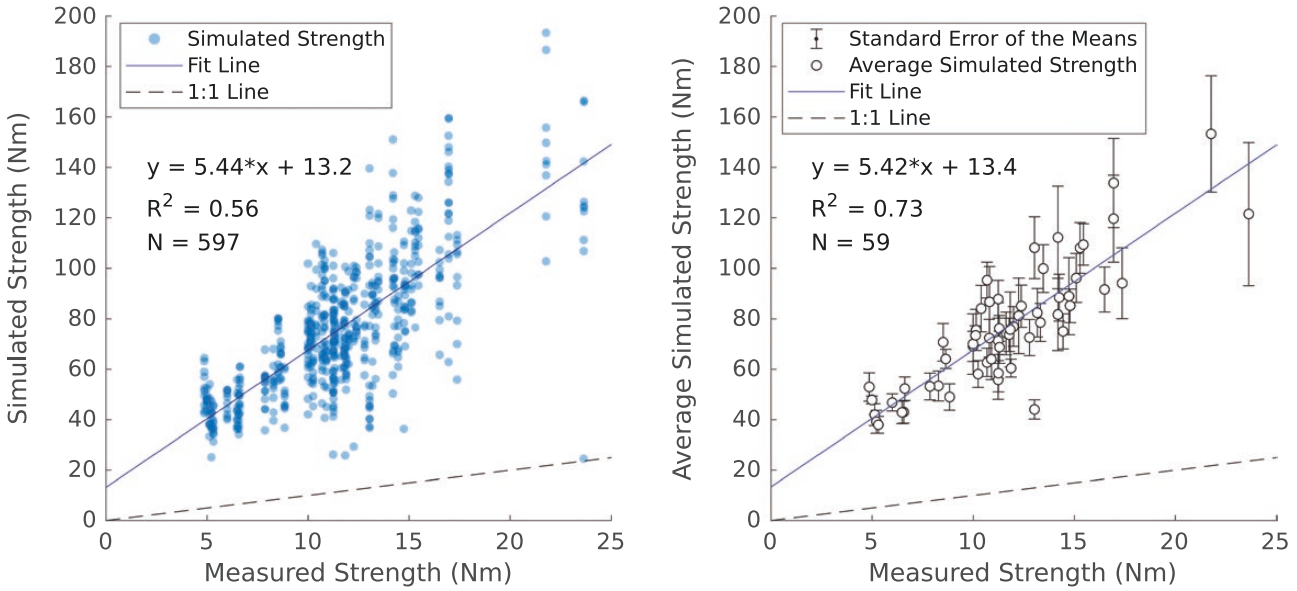

Figure 8. Comparisons between measured flexural stiffness (horizontal axis) and predicted flexural stiffness (vertical axis). The left-hand panel depicts the individual values obtained through random sampling of material properties. The right-hand panel shows the average response of each individual stalk. Error bars represent 95 % confidence intervals on the group mean for each stalk geometry.

ultimate strength was caused by material property variation. This explains the broader spread of data in Fig. 8 as compared with Fig. 7. The much stronger influence of material properties suggests that material properties have a significant effect on ultimate strength.

3.4 Assessment of the synthetic population

The synthetic population of 900 stalks exhibited nearly identical statistical characteristics as the original population, thus indicating that the Gaussian copula method can be used to create unique parameterized maize stalk models. Comparisons between the statistical characteristics of the original data set and the synthetic data set are provided in Fig. 9. As shown in the upper left-hand panel of Fig. 9, the mean parameter values of the original set were virtually identical to the mean parameter values of the synthetic data set. The same was true for the standard deviations and parameter correlation values. Finally, term-by-term comparisons of the original and synthetic cumulative density functions were also very similar (lower right panel of Fig. 9).

The similarities between the original and synthetic data sets were further visualized by comparing the probability density distributions and scatter plot relationships of four representative parameter pairs. The scatter plot relationships between these parameter pairs along with the distributions of each parameter are shown in Fig. 10. Both the original data (open circles) and the synthetic data (orange dots) are depicted. This figure illustrates the high degree of similarity between the original and synthetic data sets.

4. DISCUSSION

4.1 Using the parameterized model in studies on maize biomechanics

The parameterized model can be used in two main ways. First, the model can be used to provide a close approximation to the geometry of a real maize stalk. This is accomplished by obtaining empirical profiles for the major diameter, minor diameter and rind thickness. Landmark points are then identified on the actual stalk and matched by the parameterized model. Finally, transitions between landmark points are captured by performing least-squares regressions on the transition pattern of the real stalk with the series of empirical eigenfunctions of the parameterized model as the basis functions.

The specimen-specific 'fitting' approach requires detailed geometric information on the stalk to be modelled. Such data could be obtained from a CT scan or from photographs. Once the parameterized model has been used to match a physical specimen, the behavior of the specimen-specific model can be simulated. In addition, the model can be modified to assess the sensitivity of the specimen to hypothetical changes in geometry and material properties. Alternatively, optimization can be performed, using the specimen-specific model as a starting point.

Previous studies have reported that maize stalk morphology has a strong effect on stalk strength (von Forell *et al.* 2015; Robertson *et al.* 2017, 2022). However, those studies examined gross anatomical features such as major diameter, minor diameter, rind thickness and section modulus. The much finer control over stalk morphology enabled by this new model will allow previous results to be further decomposed. This will help us determine precisely which morphological changes could provide the greatest increase in strength for the smallest overall change in morphology and overall stalk mass.

The second approach is to create synthetic stalk populations without the need for specimen-specific data. This is done by specifying the set of 51 parameter values. In this approach, the chosen values must be mutually compatible, and profiles should be representative of actual maize stalks. However, the data that were used to create the parameterized model can be used as a starting point.

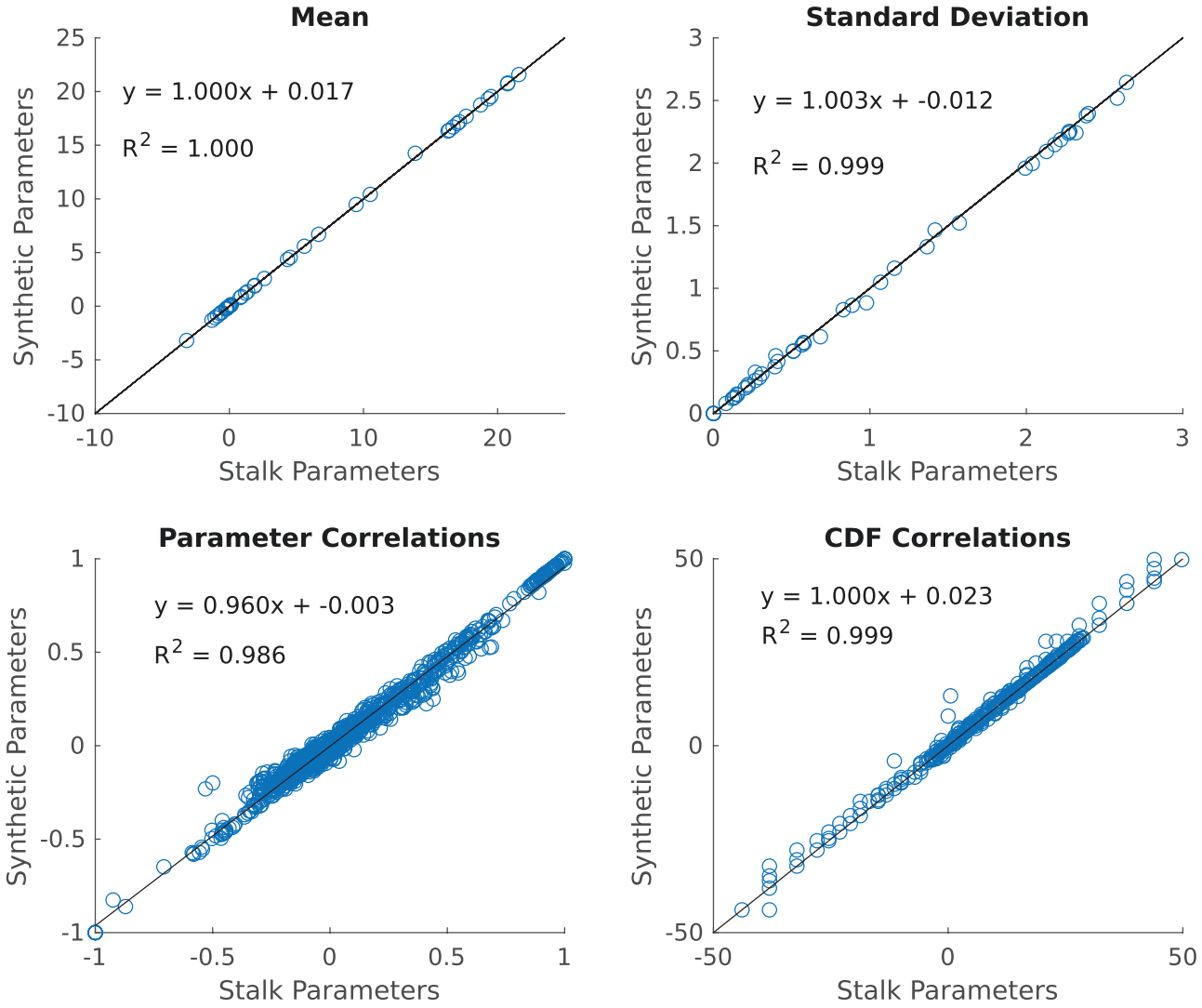

Figure 9. Scatter plots depicting the statistical similarities between empirical parameters (horizontal axes) and synthetic parameters (vertical axes).

4.2 Using this approach to model other grain species

All grains rely upon a similar geometric architecture. Thus, it may be possible to directly apply the parameterized model developed in this study to other grain species such as sorghum, wheat, oats, and rice. More research would be needed to determine the applicability of this model to other species. Alternatively, the methods described in this study could certainly be used to develop a parameterization that is unique for each grain species.

4.3 Model limitations and future improvements

The model described in this study captures gross anatomical features, but does not model smaller features such as internal vascular bundles, internal transitions between internodes and the tendency of the stalk cross-section to change dramatically when primary or secondary ears are developed. Additional research will be needed in these areas.

This model relies upon the assumption that each cross-section of the stalk is purely elliptical. In our previous research, we showed that this assumption provides a favourable balance between model complexity and predictive power. In some loading conditions, the presence of the ear groove may be necessary to accurately predict stalk mechanics. If the ear groove is needed, additional modelling efforts would be required to add a parameterized ear groove to the model. We previously described a parameterized cross-sectional model of the maize stalk that includes the ear groove and other minor geometric factors. That model could be combined with the model in this paper to simulate the ear groove with relatively high fidelity.

This model assumes that the maize stalk can be accurately modelled using two distinct tissue types: rind and pith. In reality, the boundary between rind tissue and pith tissue is gradual rather than distinct. More research would be needed to capture the functionally graded aspect of maize stalks, but the exterior shape of the gross anatomy provided by the model outlined in this paper could be used as a starting point for such a model.

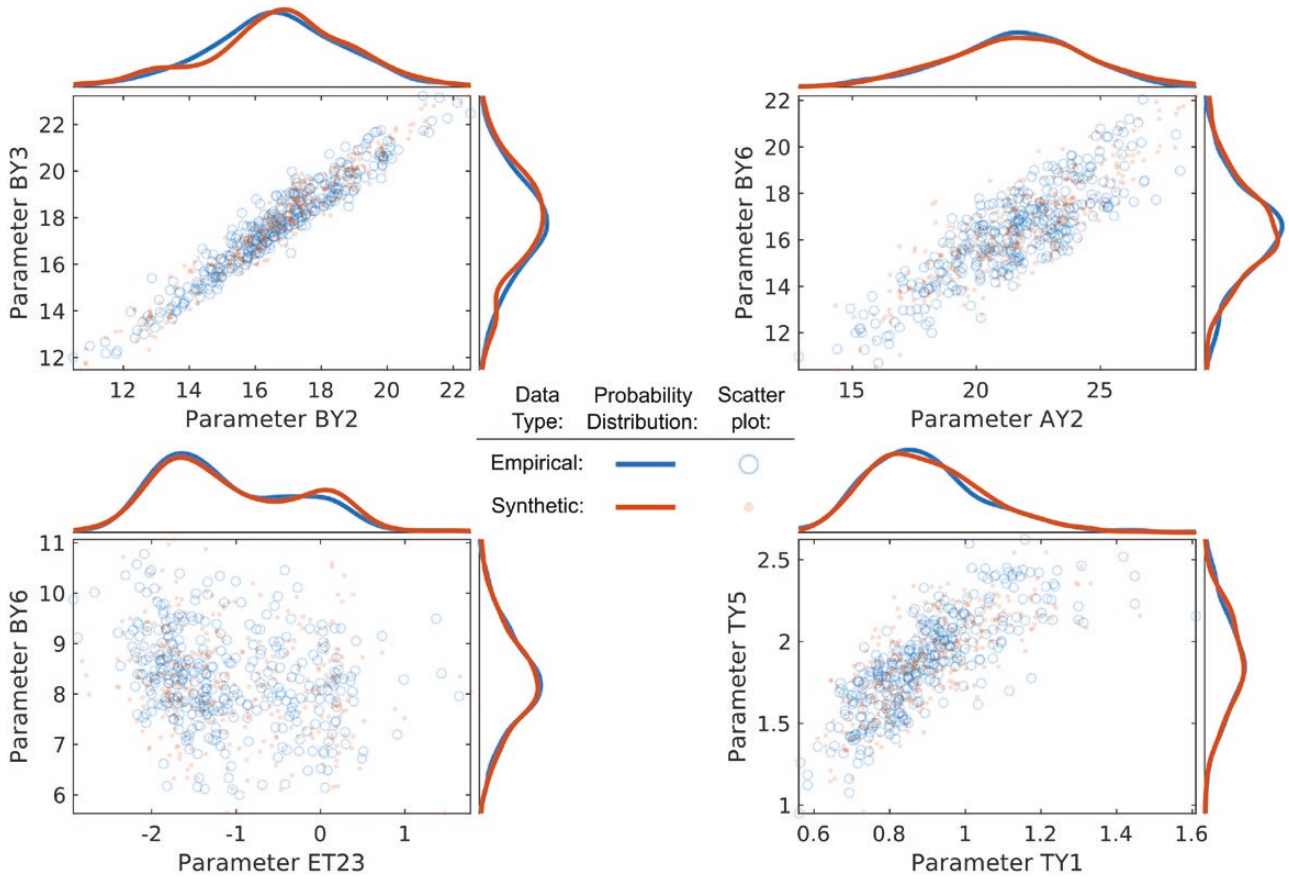

Figure 10. Histograms and scatter plots for four selected parameters from the original (blue, open circles) and synthetic (orange, dots) data sets.

5. CONCLUSION

This study provides a major improvement over the time-consuming process previously required to create specimen-specific models of maize stalks. As evidenced by validation data, this new model accurately captures the behaviour and trends observed in empirical tests of maize stalks. Most importantly, this new model allows individual physical features of the maize stalk to be independently controlled, thus opening the door to future studies focused on geometric sensitivity analysis, optimization studies and the creation of synthetic populations of maize stalks for future study.

SUPPORTING INFORMATION

The following additional information is available in the online version of this article –

Table S1. List of all parameters needed to define a unique 3D maize stalk model. Refer to Figure 4 of the paper for a diagram of landmarks and eigenfunctions.

SOURCES OF FUNDING

This research was supported by a National Science Foundation CAREER Award (#2046669).

CONFLICT OF INTEREST STATEMENT

None declared.

CONTRIBUTIONS BY THE AUTHORS

N.W.L. identified landmarks, created the landmark identification algorithm and created the process used to convert profile paths to solid models. M.O. performed the initial principal component analysis (PCA) and integrated PCA results with landmarks to produce parameterized profile paths. J.C. created the code used to automate the creation of finite element models and performed the finite element analyses. R.H. integrated and revised the codes created by M.O. and N.W.L. so that they could be used in an automated manner. D.C. supervised each stage of the project. All authors were involved in the writing of the manuscript.

ACKNOWLEDGEMENTS

The authors specially thank Dr Christopher Stubbs for providing advice and guidance on finite element modelling procedures.

AVAILABILITY OF DATA AND MODELS

We encourage other researchers to use the parameterized maize stalk model. While the model is not currently available in an online format, the model and data used in this study are available from the corresponding author upon reasonable request.

REFERENCES

Al-Zube L, Robertson DJ, Edwards JN, Sun W, Cook DD. 2017. Measuring the compressive modulus of elasticity of pith-filled plant stems. *Plant Methods* 13:1–9. doi:10.1186/s13007-017-0250-y.

Al-Zube L, Sun W, Robertson D, Cook D. 2018. The elastic modulus for maize stems. *Plant Methods* 14:11. doi:10.1186/s13007-018-0279-6.

Andersen MS, Dzialo CM, Marra MA, Pedersen D. 2021. A methodology to evaluate the effects of kinematic measurement uncertainties on knee ligament properties estimated from laxity measurements. *Journal of Biomechanical Engineering* 143:061003–061003-7. doi:10.1115/1.4050027.

Besnault B, Lavaste F, Guillemot H, Robin S, Le Coz J-Y. 1998. A parametric finite element model of the human pelvis. *SAE Transactions* 107:2680–2694.

Bolton T. 2020. Buckling analysis of sandwich composite cylindrical-conical shells. https://repository.tudelft.nl/islandora/object/uuid%3Adf9f858f-cb75-47f8-8342-a64da55f0f5f

Cook D, Julias M, Nauman E. 2014. Biological variability in biomechanical engineering research: significance and meta-analysis of current modeling practices. *Journal of Biomechanics* 47:1241–1250.

Danelson KA, Loftis KL, Yu MM, Gayzik FS, Geer CP, Stitzel JD, Slice DE. 2009. Geometric shape scaling factors for the pediatric brain based on morphometric analysis. *SAE International Journal of Passenger Cars - Electronic and Electrical Systems* 1:605–611.

Duvick DN. 2005. The contribution of breeding to yield advances in maize (*Zea mays* L.). In: *Advances in agronomy*, Vol. 86. Cambridge, MA: Academic Press, 83–145. doi:10.1016/S0065-2113(05)86002-X.

Erdemir A, Viveiros ML, Ulbrecht JS, Cavanagh PR. 2006. An inverse finite-element model of heel-pad indentation. *Journal of Biomechanics* 39:1279–1286. doi:10.1016/j.jbiomech.2005.03.007.

Flint-Garcia SA, McMullen MD, Darrah LL. 2003. Genetic relationship of stalk strength and ear height in maize. *Crop Science* 43:23.

Gomez FE, Muliana AH, Niklas KJ, Rooney WL. 2017. Identifying morphological and mechanical traits associated with stem lodging in bioenergy sorghum (*Sorghum bicolor*). *Bioenergy Research* 10:635–647. doi:10.1007/s12155-017-9826-7.

Green DW, Winandy JE, Kretschmann DE. 1999. Mechanical properties of wood. In: *Wood handbook—wood as an engineering material. General Technical Report FPL-GTR-190*. Madison, WI: US Department of Agriculture, Forest Service, Forest Products Laboratory. 5–1, 5–46. https://www.fpl.fs.usda.gov/documnts/fplgtr/fplgtr190/

Jackson JE. 2003. *A user's guide to principal components*. Hoboken, NJ: Wiley-Interscience.

Jun XUE, Xie R, Zhang W, Wang K, Peng HOU, Bo M, Ling GOU, Shaokun LI. 2017. Research progress on reduced lodging of high-yield and-density maize. *Journal of Integrative Agriculture* 16:2717–2725.

Kolodiazhnyi K. 2020. *Hands-on Machine Learning with C++: Build, train, and deploy end-to-end machine learning and deep learning pipelines*. Packt Publishing Ltd.

Lempriere BM. 1968. Poisson's ratio in orthotropic materials. *AIAA Journal* 6:2226–2227.

Maurel N, Lavaste F, Skalli W. 1997. A three-dimensional parameterized finite element model of the lower cervical spine, study of the influence of the posterior articular facets. *Journal of Biomechanics* 30:921–931.

McClarren RG, McClarren, & Penrose. 2018. *Uncertainty quantification and predictive computational science*. Springer.

Nelson N, Stubbs CJ, Larson R, Cook DD. 2019. Measurement accuracy and uncertainty in plant biomechanics. *Journal of Experimental Botany* 70:3649–3658.

Ottesen MA, Larson RA, Stubbs CJ, Cook DD. 2022. A parameterised model of maize stem cross-sectional morphology. *Biosystems Engineering* 218:110–123.

Patil DD, Deore SG. 2013. Medical image segmentation: a review. *International Journal of Computer Science and Mobile Computing* 2:22–27.

Robertson D, Smith S, Gardunia B, Cook D. 2014. An improved method for accurate phenotyping of corn stalk strength. *Crop Science* 54:2038–2044.

Robertson DJ, Brenton ZW, Kresovich S, Cook DD. 2022. Maize lodging resistance: stalk architecture is a stronger predictor of stalk bending strength than chemical composition. *Biosystems Engineering* 219:124–134. doi:10.1016/j.biosystemseng.2022.04.010.

Robertson DJ, Julias M, Lee SY, Cook DD. 2017. Maize stalk lodging: morphological determinants of stalk strength. *Crop Science* 57:926–934. doi:10.2135/cropsci2016.07.0569.

Robertson DJ, Lee SY, Julias M, Cook DD. 2016. Maize stalk lodging: flexural stiffness predicts strength. *Crop Science* 56:1711–1718. doi:10.2135/cropsci2015.11.0665.

Robertson DJ, Smith SL, Cook DD. 2015a. On measuring the bending strength of septate grass stems. *American Journal of Botany* 102:5–11.

Robertson DJ, Julias M, Gardunia BW, Barten T, Cook DD. 2015b. Corn stalk lodging: a forensic engineering approach provides insights into failure patterns and mechanisms. *Crop Science* 55:2833–2841.

Sher A, Khan A, Cai LJ, Ahmad MI, Asharf U, Jamoro SA. 2017. Response of maize grown under high plant density; performance, issues and management-a critical review. *Advances in Crop Science and Technology* 5:1–8.

Sigal IA, Yang H, Roberts MD, Downs JC. 2010. Morphing methods to parameterize specimen-specific finite element model geometries. *Journal of Biomechanics* 43:254–262.

Stubbs CJ. 2019. *Computational modeling of maize stems*. New York, NY: New York University.

Stubbs CJ, Baban NS, Robertson DJ, Al-Zube L, Cook DD. 2018. Bending stress in plant stems: models and assumptions. In: Geitmann A, Gril J, eds. *Plant biomechanics—from structure to function at multiple scales*. Cham, Switzerland: Springer Verlag, 49–77. https://www.springer.com/gp/book/9783319790985

Stubbs CJ, Larson R, Cook DD. 2020. Mapping spatially distributed material properties in finite element models of plant tissue using computed tomography. *Biosystems Engineering* 200:391–399. doi:10.1016/j.biosystemseng.2020.10.008.

Stubbs CJ, Larson R, Cook DD. 2022. Maize stalk stiffness and strength are primarily determined by morphological factors. *Scientific Reports* 12:1–11.

Stubbs CJ, Sun W, Cook DD. 2019. Measuring the transverse Young's modulus of maize rind and pith tissues. *Journal of Biomechanics* 84:113–120.

Von Forell G, Robertson D, Lee SY, Cook DD. 2015. Preventing lodging in bioenergy crops: a biomechanical analysis of maize stalks suggests a new approach. *Journal of Experimental Botany* 66:Article 14. doi:10.1093/jxb/erv108.

Xu J, Zhao Q, Qiao P. 2013. A critical review on buckling and post-buckling analysis of composite structures. *Frontiers in Aerospace Engineering* 2:157.

Zhang L, Yang Z, Zhang Q, Guo HL. 2016. Tensile properties of maize stalk Rind. *BioResources* 11:6151–6161. doi:10.15376/biores.11.3.6151-6161.